Proceedings of the 2003 IEEE International Frequency Control Symposium and PDA Exhibition
Jointly with the 17th European Frequency and Time Forum

3-D MODELING OF HIGH-Q QUARTZ RESONATORS FOR VHF-UHF APPLICATIONS

M. K. Lim[1], R. T. M'Closkey[1], D. Kirby[2], R. Kubena[2], J. R. Vig[3], A. Ballato[3], Y. K. Yong[4]
[1]Mechanical & Aerospace Engineering Dept., University of California, Los Angeles, CA, USA
[2]HRL Laboratories, Malibu, CA, USA
[3]U.S. Army CECOM, Ft. Monmouth, NJ, USA
[4]Civil & Enviromental Engineering Dept., Rutgers University, NJ, USA

Abstract - **This paper presents the optimized design and analysis of a new circular quartz resonator for VHF-UHF filtering applications. The resonator is designed for ease of packaging and integration with on-chip electronics using a new quartz-MEMS process that is being developed at HRL Laboratories. A key feature of this design is the removal of the metal electrodes from the active regions in order to enhance the mechanical gain. As an example of this design, we have modeled a 9.8µm thick circular plate (383-µm-diameter) with a 10-µm-thick double-sided circular resonator as the active region. The 200 µm diameter resonator has a 0.1 µm step above each face of the plate. The entire structure is composed of AT-cut quartz. This design provides a high degree of energy trapping for the fundamental thickness-shear mode at approximately 168 MHz. Around the resonator on each face of the plate is a pair of opposing 600 Å-thick annular Al electrodes. The width of the electrodes is 40 µm and a 1.5 µm gap exists between the inner edge of the electrodes and the central areas. We will present numerical results showing that this electrode arrangement provides effective acoustic coupling to the thickness shear mode of the central resonator area. A frequency sweep provides a plot of the motional impedance of the resonator and is a very effective tool for assessing the acoustic coupling between the electrodes and TS mode as function of the electrode-mesa gap. We will also demonstrate a trade-off between Au and Al electrodes for this design.**

Keywords- **UHF quartz resonator, Electrode free resonator design, High Q resonator.**

I. INTRODUCTION

Many of today's applications require ultra-small and ultra-low-power transceivers and signal processors. Their central component is a resonator which can be a piezoelectric material like quartz or an electrical circuit. For such application requirements, the resonator must have an excellent quality factor, be highly stable, and be able to operate at ultra high frequency. Current UHF resonators cannot meet all these requirements. For example, there are 1GHz SAW resonators but their Qs in general are poorer than BAW resonator [1]. For oscillators, there are readily available 150MHz resonators that use a multiplying circuit to obtain 600MHz frequencies. However, the added complexity in the electronics consumes more power and requires more space. In general, it is also less stable and noisier [1], [2], [7].

The stringent requirements have created a new set of issues ranging from effects of boundary conditions to manufacturing challenges. For example, a 1.2GHz thickness shear quartz resonator is about 1.25µm thick. Plating two 0.1µm thick electrodes onto its surfaces increases the total thickness by about 17%. On the other hand, adding the same set of electrodes onto a 100µm thick resonator is only about 0.2% of the total thickness. As a consequence, a resulting frequency shift of the 1.25µm quartz plate for a given amount of electrode film stress would be over 80 times larger than a 100µm quartz plate [12]. Likewise, many boundary effects such as thermal expansion mismatch between different materials[2], energy dissipation through electrodes [5], adsorption and desorption of contaminants [6] would be magnified.

Two 620MHz quartz resonators have been recently reported. In 1998 Ishii et al manufactured a 2.5µm thick 620MHz AT-Cut quartz resonator with a Q of 2,320 [3]. Their resonator was based on a strip resonator design in which the electrode was placed on the active region for both driving and sensing, and energy trapping. Yamada et al also manufactured a similar 620MHz resonator which has a Q of about 4,000 [2].

This paper will present a new electrode-free quartz resonator design that will greatly reduce the impact of the electrode on the mode of interest. Without the interference of the electrode, we anticipate a Q of 50,000 for a 500 MHz resonator [1]. This paper focuses on optimizing a 168 MHz version of this design which is currently being manufactured by HRL Laboratories. In the near feature, a UHF version will be designed and manufactured.

Energy trapping, motional resistance, and acoustic coupling are explored and optimized through adjusting acoustic gap, electrode width, and amount of mass loading of the electrode. We use a beta release of a commercial FEA package from Coventor for this analysis.

II. 3-D MODELING TOOL

The finite element analysis (FEA) software is capable of analyzing 3D piezoelectric structures, yielding mode shapes and motional impedance versus frequency. A beta version of the software was benchmarked against analytical solutions available in published literature and against the measurement data of a Statek quartz resonator. The favorable comparison verified that the software can be

used for design studies with confidence. This Statek benchmarked is discussed next.

Impedance measurement data from Statek [9] on a production rectangular AT-cut quartz resonator which operates at a 10 MHz fundamental thickness shear model is shown in Figure 1. We modeled the essential dimensions of the resonator (L1496µm, W5715µm, and T162.7µm) and electrode dimension and location and compared it to the data obtained with an Agilent 4294A. A characterization of both impedance curves using equivalent circuit model was performed. These circuit elements are listed in Table 1. The two curves are close but the numerical computed curve shows more activity in frequency range above the fundamental shear mode. This is most likely due to modifications of the production resonator (with the purpose suppressing anharmonic modes and overtones) that are not incorporated into the FEA model.

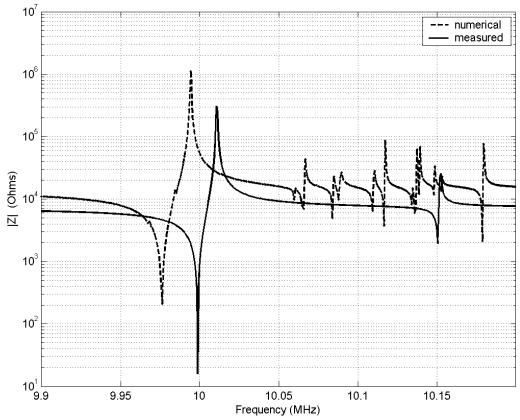

Fig. 1. Impedance magnitude plots of Statek resonator (solid) and FEA (dash).

TABLE 1
EQUIVALENT CIRCUIT ELEMENTS OF A STATEK STRIP RESONATOR AND FEA MODEL

	Statek	FEA
C_o	2.24 pF	1.17 pF
C_1	5.45 fF	4.36 fF
R_1	15.5 Ω	75.5 Ω
Q	220,000	100,000

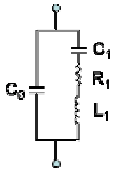

Table 1 shows good agreement between the measurements and analysis. The packaging capacitance, which is present in the Statek resonator, is not included in the model. This explains the difference in the off-resonance magnitudes. The Q difference between the physical resonator and the model is the explanation for the discrepancy between the motional resistances. A Q of 100,000 was selected for the FEA, however, the Statek resonator Q is closer to 220,000. Therefore, the motional resistance, R_1, of the Statek resonator is smaller than the motional resistance of the model. In light of the understanding that there are inherent differences between the model and the actual device, the comparison actually indicates a better agreement than at first glance.

III. ELECTRO-FREE RESONATOR DESIGN

A. Physical Description

Figure 2 shows both top and cross-sectional view of the electrode-free resonator design. The top and bottom sides of the resonator are symmetrical. The layout of the design is a circular depression situated on both major faces of a square quartz plate. In each depression, there is a circular platform. The platform is the active region of the structure and is called the center resonator area (CRA). For sensing and excitation, a circular ring electrode on each face of the plate is placed around the CRA.

For our nominal design, the thickness, t_2, of CRA is 10µm and its diameter, d_3, is 200µm. The thickness of the plate, t_2, is 9.8µm and its diameter, d_2, is 383µm. The width of the electrode, W_1, is 40µm and its thickness, t_1, is 600Å. The acoustic gap, l_1, separating CRA and the inner radius of the electrode is 1.5µm. Adjustments are subsequently made on these values. The part labeled 'mesa' adds more structural integrity to the plate. Its thickness is 25µm.

The device is designed so that the majority of the energy of the TS mode is confined to the CRA. This is done by making the CRA 0.2µm thicker than the plate (0.1µm step on each side). The CRA acoustically couples to the electrode for both sensing and driving.

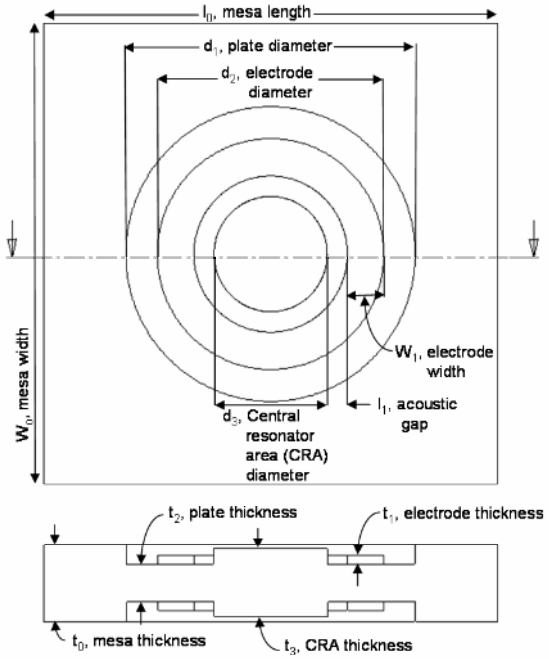

Fig. 2. Electrode-free resonator design. (not to scale: features are exaggerated for clarity). The inner most circle is referred to as *circular resonator area* (CRA).

B. Modeling

In the finite element analysis, the mesa is replaced with clamped boundary condition on the outer edge of the plate in order to simplify analysis. The thickness of the electrode is smaller than the resonator step height and it is modeled with one element. As a consequence, the electrode contributes primarily to mass loading in the analysis. The energy dissipated in the resonator is modeled using the Raleigh modal damping [11]. The two parameters in the Raleigh damping model are chosen so that the quality factor of the resonator is 100,000 in a neighborhood of the TS mode.

IV. RESULTS

A. Fundamental Thickness Shear Mode

The fundamental thickness shear mode for the nominal design is shown in Figure 3. The modal displacement of this mode can be readily seen by looking at the cross sectional view of the resonator in Figure 3. A 10μm thick central area results in a 169 MHz shear mode. Because of the height difference between the plate and resonator, the majority of the TS energy trapped within the central resonator area which functions as a resonance cavity. The isometric view reveals wavelike features on the surface of the resonator. These are the flexural components of the shear mode and they will be addressed in a later section.

The novel feature of this design is the placement of the electrode off the active region. Less charge, however, will be developed on the electrode which will lead to higher motional resistance. The next study reveals the extent to which the motional resistance and coupling coefficient are affected. Exploration and optimization are performed to achieve better understanding of the design.

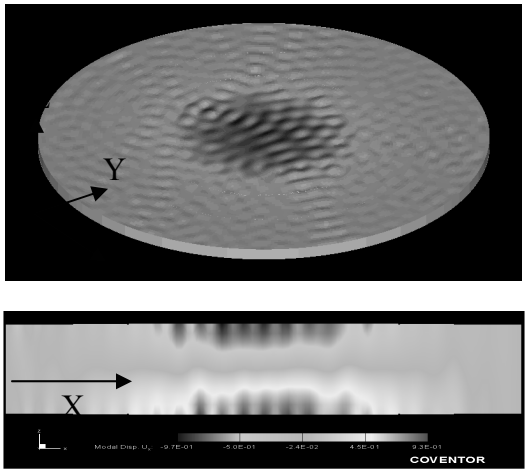

Fig. 3. Fundamental thickness shear mode of the electrode-free resonator design. The dark region signifies large displacements in the x-direction. Top: isometric view where flexure is visible. Bottom: cross-sectional view along the x-axis.

B. Motional Resistance

This study reveals how the electrode-free resonator design performs in relation to a conventional design in which the electrodes are located on the resonator. This is accomplished by taking the nominal design and driving it in two different ways. In the first method, both driving and sensing are done through the circular ring electrodes. In the second method, a potential is applied directly across the center region. Unlike a real experiment, this can be implemented easily in FEA by using a set of massless electrodes. The charge developed on them will then be measured.

As expected, the conventional design has smaller motional resistance because the charge is measured from areas which have a strong presence of the shear motion. Figure 4 shows its motional resistance, the minimum point on the impedance curve, to be 13Ω. In contrast, the charge that develops on the circular ring electrodes is from exponentially decaying shear motion thus leading to a higher motional resistance. From Figure 4, the motional resistance of this design is about 80Ω, which is still an acceptable level. The coupling coefficient, k, is 0.09 for the conventional resonator, respectively 0.02 for the electrode-free design.

C. Motional Resistance versus Acoustic Gap

This study quantifies the motional resistance and the coupling coefficient of the design as a function of the acoustic gap. The acoustic gap of the nominal resonator is varied from 1.5μm to 15μm. In order for the static impedance of each design to stay constant, the electrode surface areas of each case are made equal by adjusting the outer radius of the electrode. This gives a better comparison between cases. The impedance curves which are plotted in Figure 5 show that the motional resistance of the 1.5μm case is about 80Ω and the 15μm case is about 220Ω. A 10 fold increase in gap size leads only to about 3 fold increase in motional resistance. This realization is very beneficial from the manufacturing point of view because the acoustic gap can be manufactured with looser tolerance without severely affecting the motional resistance. Figure 6 summarizes the trend of both motional resistance and coupling coefficient versus acoustic gap.

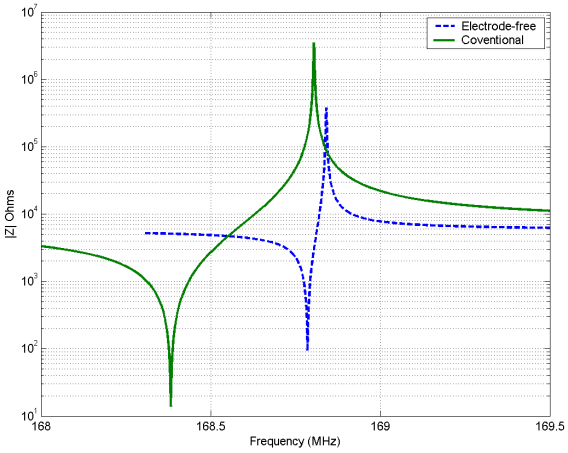

Fig.4. Impedance magnitude plots of the conventional resonator design versus the electrode-free resonator design.

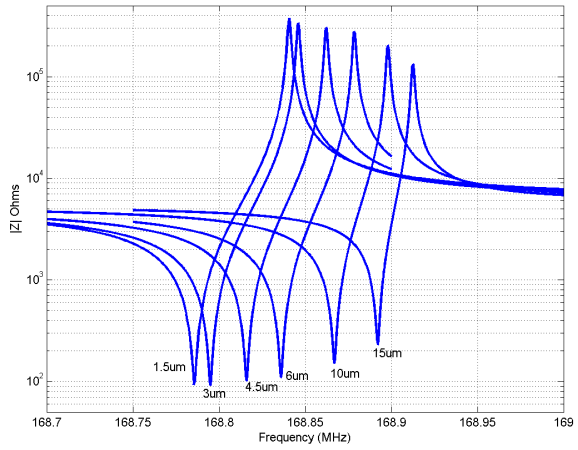

Fig. 5. Impedance magnitude plots of design with different gaps.

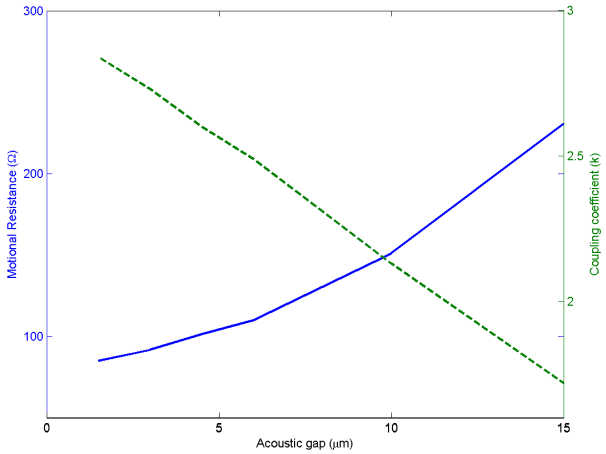

Fig. 6. A summary of motional resistance and coupling coefficient versus acoustic gap of Figure 5. Solid: motional resistance, dotted: coupling coefficient.

D. Aluminum versus Gold Electrode

Figure 7 shows the surface modal displacement along x-axis of two resonators. The designs are identical with the exception of the electrode material. The solid line represents the modal displacement of the resonator with aluminum electrodes and the dotted line represents the modal displacement of the resonator with gold electrodes. Dotted line shows a typical x-displacement curve of the fundamental thickness shear mode. The majority of its mechanical energy is within the center resonator area. On the other hand, the mode shape of the resonator with the gold electrode (solid line) has an anti-phase motion underneath the electrode. The gold electrode, which has a density several times larger than both aluminum and quartz, has changed the mode shape in such a way that more energy is present outside the CRA.

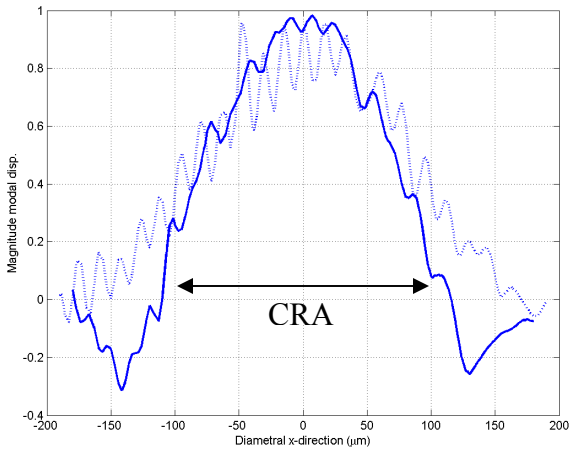

Fig. 7. Surface modal displacements along x-axis of the design with gold (solid line) electrode and aluminum (dotted line) electrode.

D. Flexure

Large displacements in the direction orthogonal to the TS particle motion are usually caused by flexural components of the TS mode. Unlike the shear motion, the flexural motion does not decay outside the CRA and as a result, interacts with the mounting structure at the boundary of the resonator. This interaction dissipates energy and should be minimized for optimizing the Q of the TS mode. One method for controlling the flexural components is to adjust the electrode width.

The mode shapes of four resonators with different electrode widths (15μm, 30μm, 40μm, and 50μm) were computed and plotted in Figures 8a-d. Their widths were varied by changing the outer radius of the electrode and maintaining a fixed acoustic gap of 1.5μm. Figures 8a-c show the x, y, and z components of TS modal displacements. Figure 8d shows the total magnitude. For a fair comparison between cases, the absolute areas under each magnitude curve in Figure 8d are made equal and then

the components in Figures 8a to 8c are scaled accordingly. Figures 8b and 8c demonstrate that flexural content varies greatly with the electrode width. The mode with 40µm electrode width has the largest Y and Z components whereas these components in the 15µm and 30µm cases exhibit the smallest amplitude. When the wavelength of the flexure, in this case approximately 15µm, is equal to, or an integer multiple of, the electrode width, the flexure magnitude is greatly reduced [10]. If the lateral dimensions of the resonators are changed, the flexure wavelength will no longer be 15µm, and a search for a new optimum electrode width is necessary.

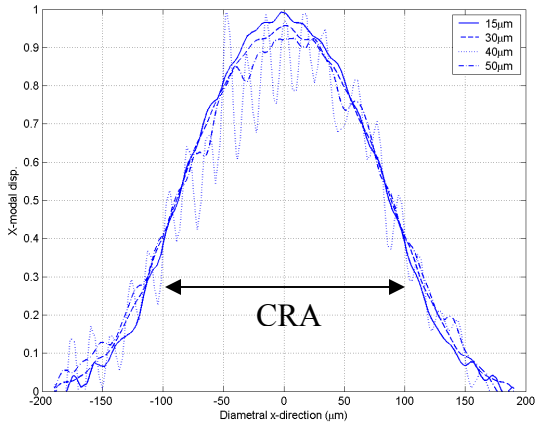

Fig. 8a. is the x-component of surface modal displacement along x-axis of resonators with different electrode widths (15µm, 30µm, 40µm and 50µm).

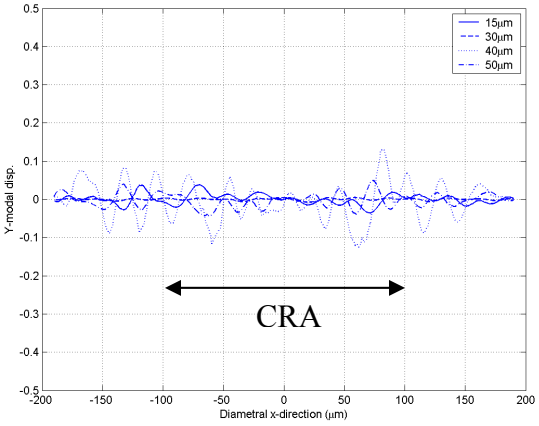

Fig. 8b. y-components of modal displacement of resonators with different electrode widths.

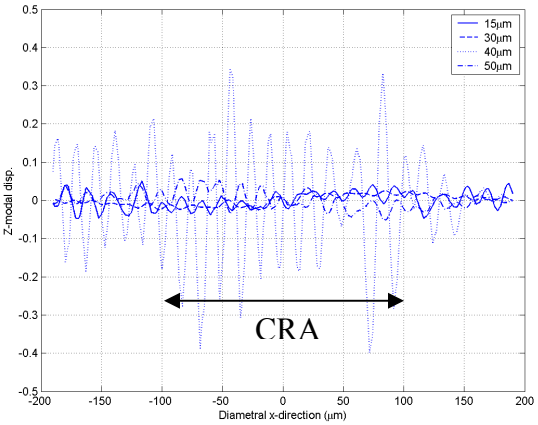

Fig. 8c. z-components of modal displacement of resonators with different electrode widths.

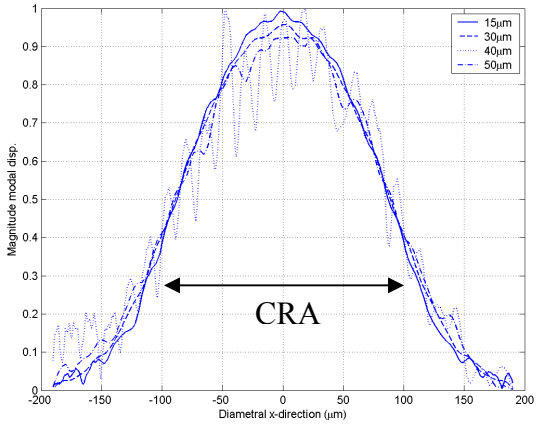

Fig.8d. Magnitude of modal displacement of resonators with different electrode widths.

E. Electrode Width Effect on Energy Trapping

Electrode width also affects the energy trapping. The wider electrode results in more surface area of the plate that is mass-loaded and as a consequence a larger amount of energy is drawn outside the resonator. Figure 9 shows a clearer picture of motion in the region outside the CRA. The 50µm case has the most energy contained outside the CRA while the 15µm case has the least energy. An electrode with zero width would give the best energy trapping, however, this would result in an infinite motional resistance. The increasing motional resistance as the electrode width is reduced is depicted in Figure 10. This trade-off will most likely have to be experimentally resolved for this class of devices due to difficulty of accurate Q modeling.

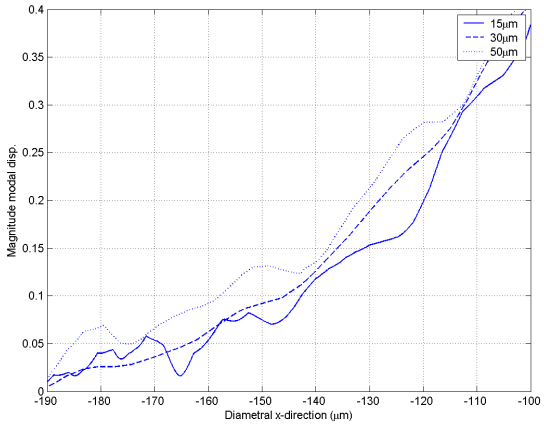

Fig. 9. An enlarged section of Figure 8d.

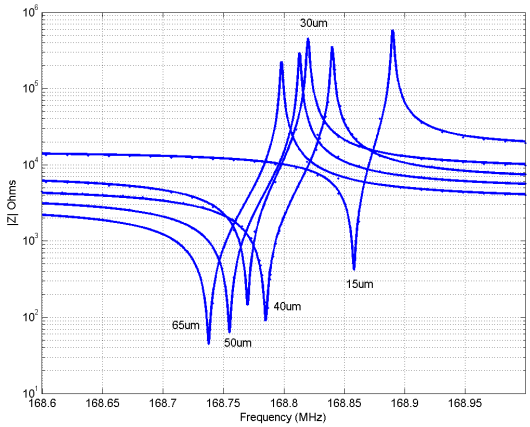

Fig. 10. Impedance of resonators with different electrode widths.

V. Conclusion

Modeling results of the electrode-free resonator have shown that it is a design worthy for use in VHF-UHF applications. With the electrode located off the active region it is anticipated that a high Q can be achieved resulting in a motional resistance of approximately 100Ω at 168MHz. A prototype that was recently manufactured is shown in Figure 11. Testing is underway and these experimental results will be reported elsewhere. There are also plans in the near future to scale this design into the ultra high frequency region.

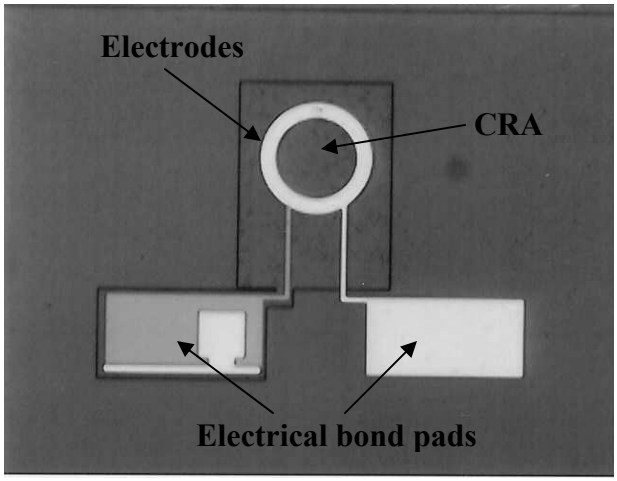

Fig. 11. Picture of a Prototype of the electrode-free resonator manufactured by HRL Laboratories.

References

[1] E. A. Gerber, T. Lukaszek, and A. Ballato, "Advances in microwave acoustic frequency sources," IEEE Trans. On Microwaves and Techniques, vol. 34, no. 10, pp. 1002-1016, October 1986.

[2] H. Yamada, H. Ura, and H. Fujiyama, "620MHz AT-Cut Fundamental crystal resonator," 2002 IEEE Int. Freq. Ctrl. Symp., pp. 174-178.

[3] O. Ishii, H. Iwata, M. Sugano, and T. Ohshima, "UHF AT-cut crystal resonators operating in the fundamental mode," 1998 IEEE Int. Freq. Ctrl. Symp., pp. 975-979.

[4] J. Kosinski, S. Mallikarjun, and A. Ballato, "Mass loading measurements of quartz crystal plates," 43rd Ann. Symp. Freq. Ctrl., pp. 365-371, 1989.

[5] R. Besson, "A new piezoelectric resonator design," 36th Ann. Freq. Ctrl. Symp. Proc., pp. 76-83, 1976.

[6] Y. K. Yong, and J. R. Vig, "Resonator surface contamination – A cause of frequency fluctuations?" IEEE Trans. Ultrason., Ferroelect. Freq. Ctrl., vol. 36, no. 4, pp. 452-458, July 1989.

[7] J. R. Vig, "Quartz crystal resonators and oscillators for frequency control and timing applications – A tutorial," January 2000.

[8] Coventor, 4001 Weston Parkway, Cary, NC 27513

[9] Statek Corporation, 512 North Main Street Orange, CA 92868

[10] Private conversation with Dr. E. P. Eernise.

[11] K. J. Bathe, Finite element procedures in engineering analysis, Prentice Hall, Inc., New Jersey, 1982, pp. 528-529.

[12] E. P. EerNisse, "Quartz resonator frequency shifts arising from electrode stress," 29th Ann. Symp. Freq. Ctrl., pp. 1-4, 1975.